Improved phase-shifting diffraction interferometer for microsphere topography measurements

Guodong Liu (刘国栋), Binghui Lu (卢丙辉), Heyi Sun (孙和义), Bingguo Liu (刘炳国)*, Fengdong Chen (陈凤东), and Zhitao Zhuang (庄志涛)

Instrument Science and Technology, Harbin Institute of Technology, Harbin 150001, China
**Corresponding author: liu_bingguo@hit.edu.cn*

Received April 25, 2016; accepted May 5, 2016; posted online June 13, 2016

In this study, an improved phase-shifting diffraction interferometer for measuring the surface topography of a microsphere is developed. A common diode-pumped solid state laser is used as the light source to facilitate apparatus realization, and a new polarized optical arrangement is designed to filter the bias light for phase-shifting control. A pinhole diffraction self-calibration method is proposed to eliminate systematic errors introduced by optical elements. The system has an adjustable signal contrast and is suitable for testing the surface with low reflectivity. Finally, a spherical ruby probe of a coordinate measuring machine is used as an example tested by the new phase-shifting diffraction interferometer system and the WYKO scanning white light interferometer for experimental comparison. The measured region presents consistent overall topography features, and the resulting peak-to-valley value of 84.43 nm and RMS value of 18.41 nm are achieved. The average roughness coincides with the manufacturer's specification value.

OCIS codes: 120.5050, 120.3180, 120.6650, 220.4830, 260.5430.
doi: 10.3788/COL201614.071202.

Microspheres are common but important objects[1,2] that are widely used in micro-mechanics and micro-optics. Higher-precision measurements of microsphere topographies are required to enable the development of micro- and nanoscale fabrication technologies. For example, small ignition-target shells are an important component in inertial confinement fusion (ICF)[3,4], and even minute defects on the surface of the target may result in failure to achieve ignition. Accurate measurements are necessary in mass production to identify the products that meet the specifications.

Atomic force microscopy (AFM), a traditional method for measuring the topography of a microsphere, requires rotating and scanning the test samples[5]. Although very high vertical resolution can be obtained, drawbacks include low efficiency and low lateral resolution between scanning paths, and isolated defects may be missed.

Interferometry possesses considerable advantages including accuracy, efficiency. and noncontact measurement capabilities[6–8]. However, most commercial interferometers are not designed for measuring microscopic objects. Lawrence Livermore National Laboratory (LLNL) developed a phase-shifting diffraction interferometer (PSDI) for ICF capsule inspection[9] that uses a short-coherence-length laser to control the interference through phase shifting. However, the high level of background light lowers the SNR, particularly when measuring low-reflectance surfaces. Therefore, in this study we present a new design for a PSDI for measuring the topography of a microsphere. This design has a higher SNR and is simpler to implement because a common laser is used.

A diagram of the PSDI is shown in Fig. 1. The linearly polarized output beam from a diode-pumped solid state laser (DPSSL) passes through a half-wave plate (HWP_1), which is used to adjust the intensity ratio. The beam is then reflected by a right-angle prism into a polarized beam splitter (PBS). The transmitted beam is used for measurements and the reflected beam is used as a reference. The beams are directed to two retroreflectors, RF_1 and RF_2. RF_2 is stationary and RF_1 is mounted on a phase shifter contained in a delay stage that provides optical path compensation. The measurement and reference beams are recombined at the PBS and then pass through a second half-wave plate (HWP_2) before being directed into a single-mode polarization-maintaining fiber (SMPMF), which is used for light transmission with vibration isolation and primary filtering. The output beam from the SMPMF is focused by an objective (L_1) onto a pinhole, which produces a nearly perfect spherical wave by diffraction. The output beam from the

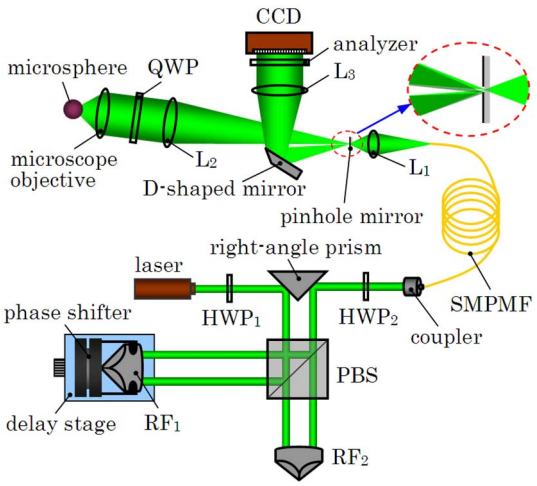

Fig. 1. Diagram of the PSDI.

pinhole is divided into two beams by a D-shaped mirror. One of these beams is reflected to a CCD sensor after passing through a collimating lens (L_3) and an analyzer. The other beam is focused on the microsphere, and the reflected light is directed to the CCD sensor by the pinhole mirror surface and the D-shaped mirror. Interference bands are formed at the CCD. By moving the phase shifter, a series of interference bands can be obtained, and this pattern is recorded using the CCD. The CCD data are processed to produce relative phase errors, and the topography of the microsphere is found by transforming the phase differences into height differences.

Unlike the LLNL interferometer, which uses a short-coherence-length laser, our interferometer uses a common DPSSL with a relatively longer coherence length. However, reflected light from the surfaces of the optical elements interferes with the signal at the CCD, so a quarter-wave plate (QWP) and an analyzer are introduced. By rotating HWP_2, the polarization of the incident light can be adjusted to coincide with the fast axis of the SMPMF so that the output beams propagating through the fiber remain linearly polarized and orthogonal. The angle between the fast axis of the QWP and the polarization direction of the measurement beam is 45°. The reflected light from the microsphere remains linearly polarized but rotated by 90°. By adjusting the analyzer transmission axis, the desired light can pass while other sources are blocked. The polarization and the propagation of the beams can be represented in the form of Jones matrices. Both the test (i.e., measurement) and reference waves are diffracted at the pinhole. The two waves can be expressed as

$$\begin{cases} E_T = \begin{bmatrix} \cos\theta \\ \sin\theta \end{bmatrix} \\ E_R = \begin{bmatrix} -\sin\theta \\ \cos\theta \end{bmatrix} \end{cases}, \tag{1}$$

where E_T and E_R are the Jones vectors for the test and reference waves, respectively, and θ is the horizontal angle for E_T. To reduce the depolarization of the reflection on the pinhole mirror surface, θ is set to zero by rotating the exit end of the SMPMF. Thus, the Jones matrices for the waves at the CCD may be expressed as

$$\begin{cases} E_{TR} = \underbrace{\begin{bmatrix} 0 & 0 \\ 0 & 1 \end{bmatrix}}_{E_A} \cdot \underbrace{\begin{bmatrix} 1 & i \\ i & 1 \end{bmatrix}}_{E_Q} \cdot \underbrace{\begin{bmatrix} re^{i\Delta} & 0 \\ 0 & re^{i\Delta} \end{bmatrix}}_{E_\Delta} \cdot \underbrace{\begin{bmatrix} 1 & i \\ i & 1 \end{bmatrix}}_{E_Q} \cdot \underbrace{\begin{bmatrix} 1 \\ 0 \end{bmatrix}}_{E_T} \\ \quad = 2re^{i\Delta}\begin{bmatrix} 0 \\ 1 \end{bmatrix} \\ E_{TD} = \underbrace{\begin{bmatrix} 0 & 0 \\ 0 & 1 \end{bmatrix}}_{E_A} \cdot \underbrace{\begin{bmatrix} 1 \\ 0 \end{bmatrix}}_{E_T} = 0 \\ E_{RR} = \underbrace{\begin{bmatrix} 0 & 0 \\ 0 & 1 \end{bmatrix}}_{E_A} \cdot \underbrace{\begin{bmatrix} 1 & i \\ i & 1 \end{bmatrix}}_{E_Q} \cdot \underbrace{\begin{bmatrix} re^{i\Delta} & 0 \\ 0 & re^{i\Delta} \end{bmatrix}}_{E_\Delta} \cdot \underbrace{\begin{bmatrix} 1 & i \\ i & 1 \end{bmatrix}}_{E_Q} \cdot \underbrace{\begin{bmatrix} 0 \\ 1 \end{bmatrix}}_{E_R} = 0 \\ E_{RD} = \underbrace{\begin{bmatrix} 0 & 0 \\ 0 & 1 \end{bmatrix}}_{E_A} \cdot \underbrace{\begin{bmatrix} 0 \\ 1 \end{bmatrix}}_{E_R} = \begin{bmatrix} 0 \\ 1 \end{bmatrix} \end{cases}, \tag{2}$$

where E_{TR} and E_{RR} are the test and reference waves reflected from the object, respectively, E_{TD} and E_{RD} are the test and reference waves reflected to the CCD directly by the D-shaped mirror, respectively, E_Q and E_A are the Jones matrices of the QWP and the analyzer, respectively, Δ is the spatial phase added by the microsphere topography errors associated with the reflectivity coefficient r, and E_Δ is the corresponding Jones matrix. Only the waves E_{TR} and E_{RD} can pass the through analyzer; the waves E_{TD} and E_{RR} are both blocked. The intensity ratio, i.e., the ratio of E_{TR} to E_{RD}, may be adjusted by rotating HWP_1, which changes the signal contrast. The phase can be altered by adjusting the phase shifter, thereby improving the contrast of the interference signal.

Because of the quasi-periodic coherence property of the laser beam[10], the optical path difference between E_{TR} and E_{RD} is minimized by moving the delay stage.

The measurement accuracy can be improved by eliminating the wave errors introduced by the optics. Fortunately, for this interferometry system most of these errors are systematic and can be eliminated by calibration. Ignoring the self-distortion of the diffracted wave, the topography data obtained by the PSDI may be expressed as

$$W = 2 \cdot (W_{MO} + W_{\mathrm{QWP}} + W_{L_2}) + W_{\mathrm{ORA}} + W_\Delta, \tag{3}$$

where W_Δ is the actual topographical measurement, W_{MO}, W_{QWP}, and W_{L_2} are the induced wave distortions for a single pass through the microscope objective (QWP and L_2), and W_{ORA} is the aberration introduced by the obliqueness of the pinhole mirror. Absolute sphericity measurements[11,12] can be made at three or five positions to determine these errors. However, it is extremely difficult to measure the same region of a sphere after a 180° rotation. Therefore, a diffracted self-calibration method was devised for calibrating the system; a diagram of the setup is shown in Fig. 2. Another the retroreflector (RF_3) is inserted between the PBS and RF_2 for directing the measurement beam to $SMPMF_2$. In this setup, HWP_3 serves the same functions as HWP_2. The output beam from a fiber collimator (FC) is modulated into a circularly polarized beam by QWP_2, and the pinhole is placed at the focal point of the microscope objective.

The test wave reflected by the object is replaced by the ideal diffraction wave from the pinhole, for which W_Δ is zero. Therefore, the resulting wave W^* can be denoted as

$$W^* = W_{MO} + W_{\mathrm{QWP}} + W_{L_2} + W_{\mathrm{ORA}}, \tag{4}$$

and from Eqs. (4) and (3), W_Δ can be expressed as

$$W_\Delta = W - 2W^* + W_{\mathrm{ORA}}. \tag{5}$$

The majority of the systematic errors are eliminated, but a residual term W_{ORA} remains. This term can be determined from the NA of E_{TR}. NA can be reduced to less than 0.05 using a long-focal-length collimating lens (L_2), in which case the peak-to-valley (PV) value of W_{ORA} is less

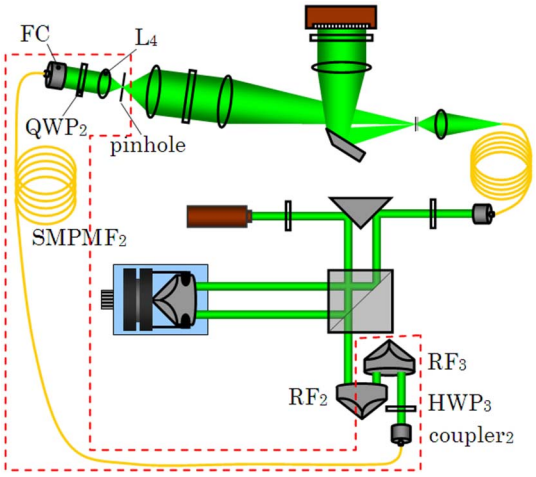

Fig. 2. Diffraction self-calibration.

than 0.0009λ[13], which is sufficiently small that it can be ignored.

The experimental setup is shown in Fig. 3; the main components are as follows: a 532 nm DPSSL, a phase shifter (resolution = 30 pm), an SMPMF (core diameter of 6 μm), an analyzer (extinction ratio 10,000:1), a microscope objective (20×, NA = 0.45, working focal distance = 5 mm), a collimating lens L_2 (focal distance = 160 mm), and a CCD (2048 pixels × 2048 pixels, pixel size of 7.4 μm). All of the components are mounted on a motorized 2D stage (PI MCS-380) for focus adjustment. A 2D rotary shaft system is mounted on a high-accuracy z axis stage for microsphere rotation and height adjustments.

The pinhole is one of the most important elements in the PSDI, and its size and roundness error determines the sphericity of the diffracted reference wavefront. Synthetically considering the aberration of diffracted wavefront and the diffraction energy efficiency, a pinhole with a diameter of 2 μm is used in our experimental setup. The pinhole is fabricated by etching its Cr film with the focused ion-beam etching (FIBE) technology and the RMS value of diffracted wavefront aberration is less than 0.0024λ over the NA 0.4, according to the scalar diffraction theory. An almost perfect round hole can be obtained with the FIBE method, so the effect of the pinhole roundness error can be negligible.

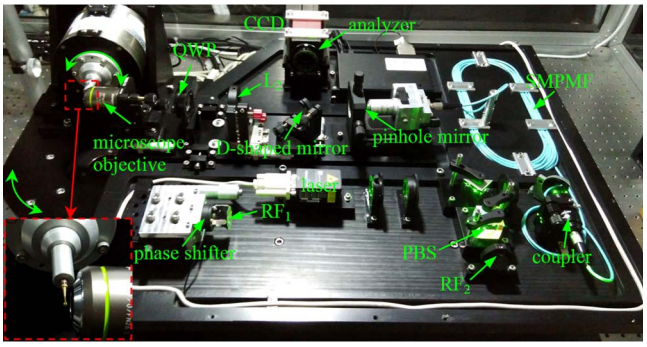

Fig. 3. Experimental setup.

The distribution of calibrated systematic errors whose PV and RMS values were 0.0557λ and 0.0081λ, respectively, is shown in Fig. 4.

A grade-5 spherical ruby tip from the stylus of a coordinate measuring machine (CMM) was used to test the interferometry system. The ruby ball had a diameter of 3 mm, a reflectivity of approximately 7.6% and a roughness (R_a) of 0.014 μm. The interference pattern and signal are shown in Fig. 5. Figure 5(a) is the original interferogram and one point on it is selected for interference signal analysis by phase shifting, whose result is shown in Fig. 5(b). The phase-shifting step length was 13.3 nm, and 140 frames were captured. From the graph, it can be observed that the contrast of the signal was approximately 0.78.

A five-frame Stoilov algorithm[14,15] was used to obtain the phase. After phase unwrapping[16,17], eccentricity error correction[18,19], and systematic errors elimination, the final topography error was obtained.

For evaluating the accuracy and proving the feasibility of our proposed system, the same region on the ruby probe was inspected by the WYKO NT1100 scanning white light interferometer (SWLI) and PSDI, respectively, as experimental comparison, and the reconstructed topography information is shown in Fig. 6. Figure 6(a) is the testing result using the SWLI, whose resulting vertical depth information has been expanded and transformed to relative profile errors, and Fig. 6(b) is the one from the PSDI system. Owing to the configuration of a 20× objective on the SWLI, its valid testing aperture and lateral resolution were a diameter of 200 and 0.4 μm, respectively, and the corresponding parameters of our PSDI were 1100 and 1.1 μm, respectively.

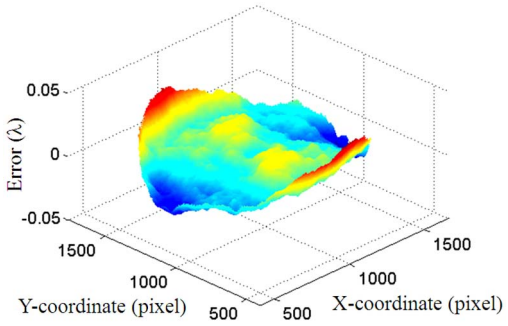

Fig. 4. Calibrated systematic errors.

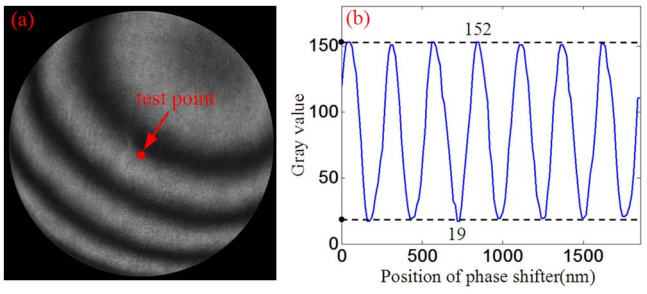

Fig. 5. Interference pattern and signal.

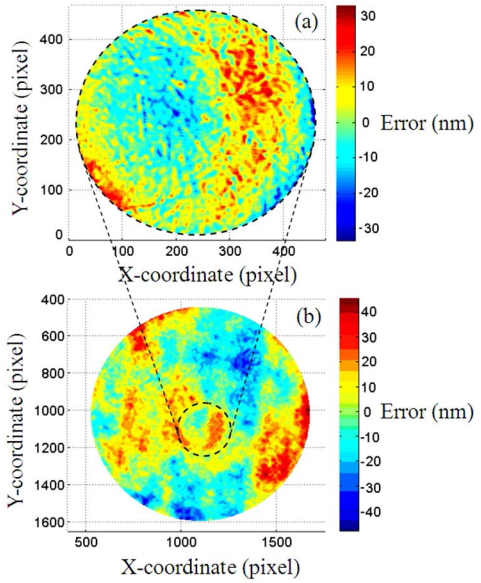

Fig. 6. Measured topographical errors.

It can be seen that the testing result with SWLI was a part of the one with PSDI, and had more detail information owing to its higher lateral resolution. However, the measured region present consistent overall topography features. The measured result comparison is shown in Table 1. The PV and RMS values on the local (compared) region with the PSDI were 66.17 and 16.89 nm, respectively, and very close to the SWLI testing result PV 64.41 mm and RMS 16.32 nm. Because of the much greater sample set, the inspecting results of the full aperture with PSDI grew to a PV of 84.43 mm and RMS of 18.41 nm.

Four symmetrical areas on the equator and one on the north pole (top) of the probe were inspected for the surface roughness test. Measurements from five locations are shown in Table 2. The PV and RMS values (R_q) were 0.1587λ and 0.0351λ, respectively. The average value of the measured surface roughness (R_a) was 0.0280λ (0.0149 μm), which coincides with the given standard value.

An improved PSDI is developed to measure the topography of microspheres. A common DPSSL rather than a short-coherence-length laser is used as the light source. The contrast in the interference bands is improved with the new optical arrangement. A pinhole diffraction self-calibration method is used to eliminate most of the systematic error. To test the PSDI system, a CMM stylus with a spherical ruby tip is used as an example. The contrast in the interference bands is as high as 0.78. The experimental result is given to confirm the accuracy and feasibility of our proposed PSDI system. The proposed system is more compact and simpler than the LLNL PSDI, and it is demonstrated that the system can accurately measure the topography of microspheres. This method is particularly useful for objects with low reflectivity.

Table 1. Measured Result Comparison.

Method	PV (nm)	RMS (nm)
SWLI	64.41	16.32
PSDI (local region)	66.17	16.89
PSDI (full aperture)	84.43	18.41

Table 2. PV, R_q, and R_a of Five Testing Locations.

Area No.	PV (λ)	RMS R_q (λ)	Roughness R_a (λ)
1	0.1589	0.0352	0.0288
2	0.1575	0.0351	0.0279
3	0.1642	0.0357	0.0286
4	0.1566	0.0348	0.0275
5	0.1561	0.0346	0.0273
Average	0.1587	0.0351	0.0280

This work was supported by the National Natural Science Foundation of China under Grant Nos. 61275096 and 51275120.

References

1. F. Zhao, M. Zhu, and P. Zhan, Chin. Opt. Lett. **8**, 119 (2010).
2. B. Shi, H. Xiao, and C. Li, Chin. Opt. Lett. **1**, 040234 (2003).
3. H. Y. Li, Y. B. Huang, S. H. E. Jiang, L. F. Jing, T. X. Huang, and Y. K. Ding, Fusion Eng. Des. **100**, 596 (2015).
4. S. X. Hu, L. A. Collins, V. N. Goncharov, J. D. Kress, R. L. McCrory, and S. Skupsky, Phys. Rev. E **92**, 043104 (2015).
5. R. Cook, G. E. Overturf, and S. R. Buckley, J. Vac. Sci. Technol. A **12**, 1275 (1994).
6. Q. Yang, B. Zhao, and X. Zeng, Chin. Opt. Lett. **11**, 021202 (2013).
7. S. Xiong, J. Liu, F. Li, P. Wang, and R. Li, Chin. Opt. Lett. **13**, 081901 (2015).
8. J. Hahn, H. Kim, Y. J. Lim, E. H. Kim, and B. Lee, Chin. Opt. Lett. **7**, 121113 (2009).
9. R. C. Montesanti, M. A. Johnson, and E. R. Mapoles, in *American Society for Precision Engineering Annual Conference 10*, UCRL-PROC-225005 (2006).
10. S. J. Li and Y. Z. Liu, Laser J. **21**, 59 (2000).
11. K. E. Elssner, R. Burrow, J. Grzanna, and R. Spolaczyk, Appl. Opt. **28**, 4649 (1989).
12. X. Hou, P. Yang, F. Wu, and Y. J. Wan, Opt. Laser Eng. **49**, 833 (2011).
13. D. Wang, Y. Yang, C. Chen, and Y. Zhuo, Acta Opt. Sin. **31**, 0612003 (2011).
14. G. Stoilov and T. Dragostinov, Opt. Lasers Eng. **28**, 61 (1997).
15. X. F. Xu and Y. P. Cao, Acta Opt. Sin. **29**, 733 (2009).
16. L. Xue, S. Wang, K. Yan, N. Sun, Z. Li, and F. Liu, Chin. Opt. Lett. **12**, 071801 (2014).
17. Y. Lu, X. Wang, X. Zhong, G. He, Y. Liu, and D. Zheng, Chin. Opt. Lett. **2**, 698 (2004).
18. D. D. Wang, Y. Y. Yang, C. H. Chen, and Y. M. Zhuo, Appl. Opt. **50**, 2024 (2011).
19. D. D. Wang, Y. Y. Yang, C. H. Chen, and Y. M. Zhuo, Opt. Commun. **284**, 3878 (2011).